THE ASTROPHYSICAL JOURNAL, 455:175–181, 1995 December 10

INTERFEROMETRIC OBSERVATIONS OF THE CIRCUMSTELLAR MOLECULAR STRUCTURE AROUND THE YOUNG STELLAR OBJECT IN L1287

JI YANG,[1,2] NAGAYOSHI OHASHI,[2,3] AND YASUO FUKUI[4]

Received 1994 January 18; accepted 1995 June 20

ABSTRACT

Results of high-resolution interferometric observations of CS (2–1) emission from the young stellar object IRAS 00338+6312 and its neighboring region in L1287 are presented. Strong and localized emission has been detected. The global CS distribution appears elongated and has a size of 0.14 pc × 0.08 pc. The CS emission shows drastically different structures at different radial velocities, including a high-velocity bipolar pattern extended over 16 km s^{-1} and a flattened structure perpendicular to the outflow axis at lower velocities. The high-velocity lobes are clumpy and have been apparently accelerated. It is found that the *IRAS* source is located in the central part of the low-velocity CS structure, while three other optical features, including the two FU Orionis candidates RNO 1B and RNO 1C, are located near or outside the edge of the low-velocity CS component. The possible driving source of the outflow in L1287 is discussed on the basis of the available data.

Subject headings: ISM: individual (L1287) — ISM: jets and outflows — ISM: molecules — stars: pre–main-sequence

1. INTRODUCTION

The dark cloud L1287 in Cassiopeia OB 14 was originally mapped in CO, HCO^+, and HCN lines by Yang et al. (1991). In the J = 1–0 lines of CO and its isotopes, the cloud appears filamentary, and the main part of the cloud contains a well-defined ^{13}CO core. This core is nearly circular, having a diameter of 1.2 pc and a mass of 130 $M_\odot$. From single-dish observations of $J = 1–0$ lines of HCO^+ and HCN at a resolution of 20″, it has been shown that a high-density core exists in the central portion of L1287. The sizes of both the HCO^+ and the HCN cores are about 0.3 pc. A lower mass limit to the core was estimated to be $\sim 10\ M_\odot$.

Within the molecular core, a molecular outflow with spatially separated velocity lobes was mapped by Snell, Dickman, & Huang (1990) and Yang et al. (1991; see also Fukui 1989). A luminous infrared source, IRAS 00338+6312, is associated with the high-density core (*IRAS* Point Source Catalog 1988) and was also identified as the driving source of the bipolar molecular outflow. This infrared source is characterized by a far-infrared luminosity of 1100 $L_\odot$ and low color temperatures, similar to those of embedded sources (Yang et al. 1991). The *IRAS* source is associated with a faint visible nebulosity. Another young stellar object which is located in the southwest of the infrared source and associated with a faint nebula, RNO 1B, was identified by Staude & Neckel (1991) to be an FU Orionis object. Along with this FU Ori object, they found two other optical maxima, RNO 1C and RNO 1D, nearby. These optical features are aligned with the axis of the CO outflow.

Kenyon et al. (1993) further reported that RNO 1C is another FU Ori star identified by comparison of near-infrared spectroscopic characteristics in RNO 1C and other FU Ori objects. They suggested that the molecular outflow in L1287 is driven by both RNO 1B and RNO 1C. On the other hand, Weintraub & Kastner (1993) pointed out that a third, deeply embedded object is responsible for the molecular outflow, as suggested by near-infrared polarization imaging. At this position, which is almost identical to the position of the *IRAS* source, Anglada et al. (1994) found a continuum source at 3.6 cm, which is associated with a single-sided thermal radio jet. The direction of this jet is parallel to the axis of the molecular outflow.

The interesting properties of the young stellar objects (YSOs) and the complicated nature of the region make L1287 deserving of further studies. We made millimeter-wave interferometric observations of IRAS 00338+6312 and its immediate neighborhood. The aims of this work are to study the molecular gas structure associated with the infrared source at higher angular resolution and to find out the possible relation between the distribution of high-density molecular gas and the embedded YSOs.

2. OBSERVATIONS

The observations were carried out with the Nobeyama Millimeter Array (NMA)[5] during 1991 April 1 and May 19. Five 10 m antennas were included in the two configurations, C and D, resulting in unprojected baselines from 6 kλ (18 m) to 40 kλ (120 m). The synthesized beam size was 7″.95 × 6″.40 in P.A. 140°. The tracking was centered at R.A.(1950) = $0^h33^m53^s.3$, decl. = +63°12′32″.0.

The observing frequency was centered at the $J = 2–1$ transition of CS at 97.981 GHz. All the antennas were equipped with 4 K cooled SIS mixer-receivers with T_{sys} in the range of 300–400 K (double sideband). The back end was a fast Fourier transform spectrocorrelator, which had a bandwidth of 80

[1] Purple Mountain Observatory, Academia Sinica, Nanjing 210008, China.
[2] Nobeyama Radio Observatory, Nobeyama, Minamisaku, Nagano 384-13, Japan.
[3] Harvard-Smithsonian Center for Astrophysics, Mail Stop 42, 60 Garden Street, Cambridge, MA 02138.
[4] Department of Astrophysics, Nagoya University, Chikusa-ku, Nagoya 464-01, Japan.

[5] This work was carried out under the common-use observation program at Nobeyama Radio Observatory (NRO). NRO, a branch of National Observatory, is a cosmic radio observing facility open for general use by researchers in the fields of astronomy, astrophysics, and astrochemistry.

MHz divided into 1024 channels and provided a velocity resolution of 0.25 km s^{-1} at the observed frequency.

Phase and amplitude calibrations were done by observing 3C 84 every 30–40 minutes during observation. At the observing frequency, the flux of 3C 84 is 7.6 Jy based on the measurements of Mars and Uranus during the observing season. The error after calibration is about 15% estimated from the statistical deviations. The complex bandpass over the 1024 channels was determined by observing 3C 84 in a period of 30–40 minutes. We used the standard CLEAN procedure of the NRAO AIPS package and adopted a natural weighting to retrieve the images. The 1 σ rms noise levels in the final maps are $\sim$170 mJy beam^{-1} for a velocity interval of 0.75 km s^{-1} in the three-channel combined line spectra and $\sim$10 mJy beam^{-1} for the continuum over the 80 MHz range.

It is sometimes the case that the synthesis observations are insensitive to the emission extended over the field of view, leading to the problem of underdetection, or missing flux. The minimum baseline is 6 kλ, or 18 m, in this observation. The allowed characteristic size for sensitive detection without significant missing flux is thus $\sim\lambda/(6\ \mathrm{k}\lambda)$, or 34″, slightly dependent on the edge taper. Referring to the size of high-density cores observed in HCN and HCO$^+$ with a single dish (Yang et al. 1991), which is about 75″, it is possible that an extended and smoothly distributed component of CS has not been detected in this observation if such a component is present. In this work we concentrate on the localized features with angular sizes of less than 40″ to which the interferometric imaging is sensitive, such as those shown in Figure 1. Measurements within this scale are believed to be less biased by the missing-flux problem.

3. RESULTS

3.1. *The Overall Emission of* CS

Strong CS emission has been detected in the velocity range between -28 and -12 km s^{-1}, and a map of this emission, along with a plot of the young stellar objects in this region, is shown in Figure 1. This map shows a localized CS structure elongated in the northeast-southwest direction, parallel to the axis of the CO outflow. The size of the emitting area, measured at the 3 σ level, is 34″ × 20″, or 0.14 pc × 0.08 pc at the source distance of 850 pc. The CS-emitting area is about one-half of that of the high-velocity CO outflow, which has a half-maximum size of 0.24 pc × 0.13 pc (Yang et al. 1991). Distribution of CS emission is not uniform. The emission peak coincides with the position of the *IRAS* source. A relatively steep edge can be found on the east and northeast sides of the total emission. In the region close to RNO 1B and extended to the west, the surface intensity can be found to be lower than average.

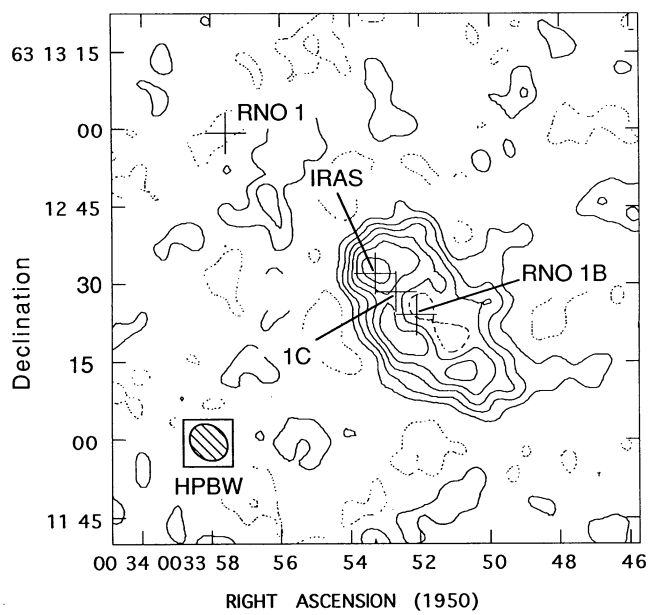

FIG. 1.—Total emission of the CS (J = 2–1) line from L1287 within the range V_{LSR} = -28 to -12 km s^{-1}. Contour levels are arranged in the order 4.10×10^{-2} (-1.5, 1.5, 3.0, 4.5, 6.0, 7.5, 9.0) Jy beam^{-1}, with an interval to be 10% of the peak intensity. Positions of IRAS 00338+6312, RNO 1C and RNO 1B are marked by crosses, in an order from northeast to southwest.

Between -17 and -19 km s^{-1}, the CS emission shows an intensity minimum with its center at $V_{LSR} = -18.00$ km s^{-1} (see also Fig. 4 below). Self-absorption may be responsible for such a minimum, as is suggested by the optically thick line profiles of HCN and HCO$^+$ (Yang et al. 1991), which may introduce ambiguity in related interpretations. But if this is the case, the self-absorption is expected to appear at $V_{LSR} = -17.00$ km s^{-1}, 1 km s^{-1} redshifted from the local rest velocity by referring to those HCN and HCO$^+$ profiles. The missing-flux problem mentioned above may also give rise to the dip in the line profile if the emission at rest velocity is rather extended. Because of the velocity coincidence of the dip with the local rest velocity, this possibility is most likely true, considering that the velocity determination is accurate within -0.25 km s^{-1}. Under such circumstances, the large-scale surface brightness distribution is hidden from the interferometric imaging, but most of the localized features with angular sizes smaller than the field of view will be faithfully reproduced.

We subtracted baselines outside the channels of CS emission and reduced the continuum component at 98 GHz. The result shows no detectable continuum emission from the field above the 3 σ limit of 30 mJy beam^{-1}. In their survey of YSOs in Taurus, Ohashi et al. (1991) find a tendency for deeply embedded sources to be mainly detected with CS line emission, but much less often at 98 GHz continuum. In contrast, visible YSOs are detected more frequently in the continuum without CS line emission. The present case suggests that the driving source of the CS outflow is deeply embedded inside dense molecular gas containing little heated dust, which produces significant CS line emission but weak radio continuum emission at 98 GHz.

3.2. *Structure of the High-Density Outflow Gas*

The large velocity interval detected from CS, 16 km s^{-1}, indicates that a significant part of CS emission comes from the outflow gas. The dynamic timescale implied by the given size and the velocity interval is 8×10^3 yr, shorter than that derived from the CO outflow (Yang et al. 1991). A drastically different distribution of the CS emission has been resolved, as shown in Figure 2. Within the velocity range $V_{LSR} = -15.50$ to -12.00 km s^{-1} the redshifted emission appears mostly north of but close to the central *IRAS* source (Fig. 2*a*), while within the range $V_{LSR} = -27.75$ to -20.00 km s^{-1} the emission shows another elongated structure, located completely to the southwest of the *IRAS* source and peaked at the far extremity (Fig. 2*c*). These two parts of the emission clearly form a bipolar pattern of dense CS outflow. Orientation of the CS outflow, estimated from the geometric weighting of the emission outlines at the 3 σ level, is close to that of CO in a position angle

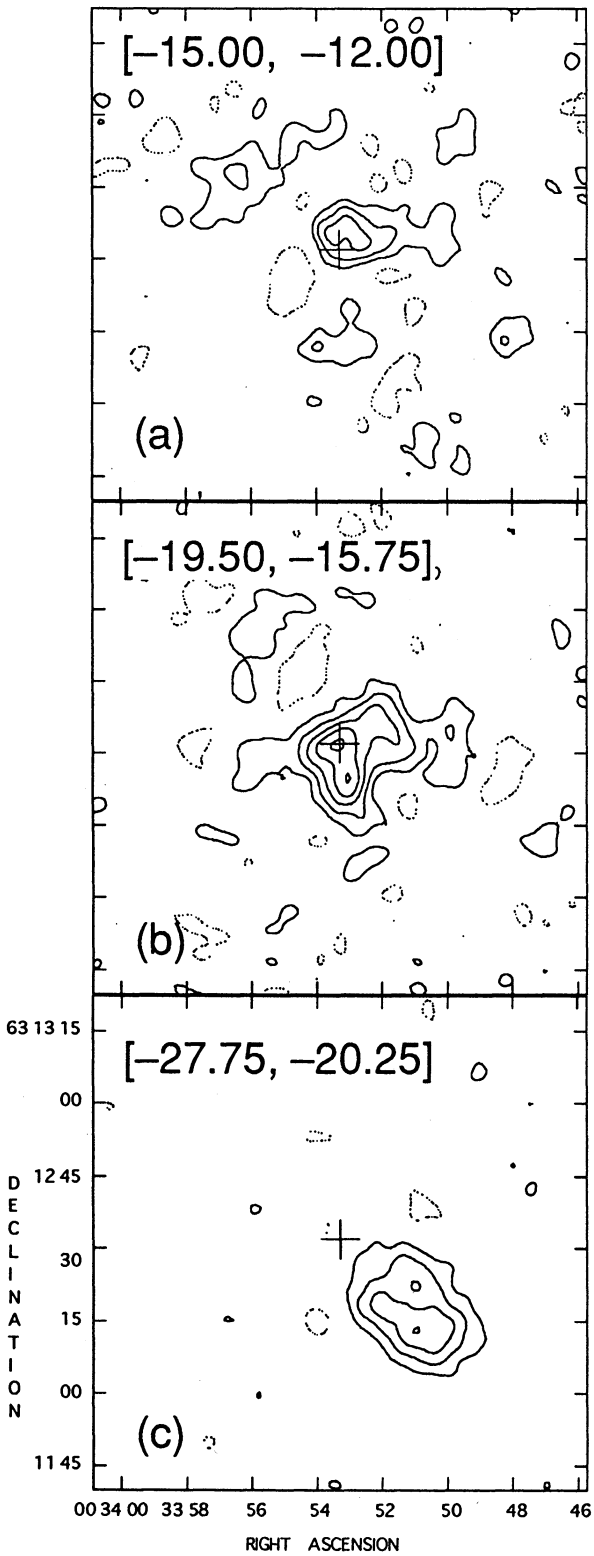

FIG. 2.—Contour maps of flux density distribution of (*a*) red, (*b*) quiescent, and (*c*) blue components. Coordinates are the same as in Fig. 1. (*a*) V_{LSR} = −15.00 to −12.00 km s^{-1}. (*b*) V_{LSR} = −19.50 to −15.75 km s^{-1}. (*c*) V_{LSR} = −27.75 to −20.25 km s^{-1}. The three panels share the same contour levels starting from −1.5 σ, or 1.14 × 10^{-2} (−1.5, 1.5, 3.0, 4.5, 6.0, 7.5, 9.0) Jy beam^{-1}. A cross in the field center marks the position of IRAS 00338+6312.

of ~45°. The positional coincidence of CO and CS outflow suggests that they are driven by the same source. The morphologies of both the CS lobes and previous maps further indicate a single driving source.

The CS outflow shows comparable velocity extension with regard to the HCO^+ wing emission at V_{LSR} = −23.8 to −13.2 km s^{-1} (Yang et al. 1991), although the clear morphology of the compact HCO^+ outflow gas was not fully resolved in the previous single-dish observations. The velocity characteristics of the CS outflow are similar to those of CO and HCO^+ from the single-dish observations (Yang et al. 1991) in the sense that the CS wings are broader on the blue side and narrower on the red. The combined results from CO, CS, and HCO^+ indicate that the outflow in L1287 is among the few cases so far observed which manifest bipolar outflow characteristics in up to three molecular species.

Some more detailed structures of the CS outflow gas have been revealed in the blue lobe. Figure 3 demonstrates the CS emission at successively decreasing radial velocities, V_{LSR} = −20 to −25 km s^{-1}. Three enhanced knots at −20.25 km s^{-1} can be identified in Figure 3*a*. This map indicates that the high-velocity flow lobe is clumpy, suggesting that molecular outflow gas contains high-density clumps in their inner portion. The expansion velocity of these clumps is lower than the gas traced by high-velocity CO emission.

From Figure 3 we find a clear tendency for the CS emission, including the clumps, to show a gradual increase of distance from the central *IRAS* source as the velocity decreases. The emission close to the central source does not appear in the velocity panel of −21.75 km s^{-1} (comparing Figs. 3*a* and 3*b*). The farthest clump extends to ~32″ (0.13 pc) southwest from the central source at V_{LSR} = −26.25 km s^{-1}. The velocity difference involved in such displacement of high-density clumps can be measured to be ~12 km s^{-1}.

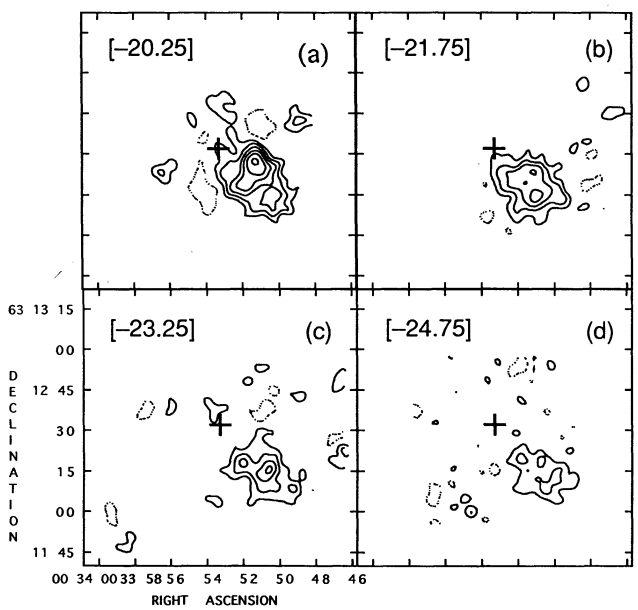

FIG. 3.—Channel maps of CS flux density at different velocities for the blueshifted outflow gas. The panel velocities are, respectively, V_{LSR} = −20.25, −21.75, −23.35, and −24.75 km s^{-1} for (*a*), (*b*), (*c*), and (*d*). The velocity width of each panel is 0.75 km s^{-1}. All the panels have the same contour levels of 1.75 × 10^{-2} (−1.5, 1.5, 3.0, 4.5, 6.0, 7.5, 9.0) Jy beam^{-1}. Marginally resolved clumps can be recognized from the panels.

In order to show more clearly the acceleration tendency of the CS outflow gas, we plotted in Figure 4 the position-velocity diagram cut along the main elongation of the outflow. From the map the velocity range of the high-velocity gas can again be traced from -26 to -14 km s^{-1}, and the minimum is clear at -18 km s^{-1}. Positional dependence of the velocity is significant for the blueshifted lobe. A linear relation between the velocity and the offset distance, $v(r) \sim r$, can be fitted over the whole CS velocity extent between -26 and -14 km s^{-1} by setting the center at the *IRAS* source, and the relation remains valid over 34″ along the outflow direction.

The outer periphery of the low-velocity CS component coincides well with the CS lobes of the outflow. We find that the *IRAS* source is located close to the center of the low-velocity structure, whereas both RNO 1B and RNO 1C are located farther away from the CS peak. The whole structure appears elongated in the direction perpendicular to the outflow axis.

3.3. *Estimation of Flow Mass*

From the luminosity of CS emission at relevant velocity intervals, we estimate the masses involved in the red, blue, and quiescent components. If we assume that the CS ($J = 2$–1) line is optically thin, the relation between CS column density and its integrated intensity will be

$$N(\mathrm{CS}) = \left(\frac{3k}{8\pi^3 \mu_{\mathrm{CS}}^2 \nu_{21}}\right)\left(\frac{2kT_{\mathrm{ex}}}{h\nu_{21}}\right) \exp\left(\frac{3h\nu_{21}}{2kT_{\mathrm{ex}}}\right) \int T_{\mathrm{A}}^{*}\, dV\,, \quad (1)$$

where ν_{10} and ν_{21} are, respectively, the frequencies of $J = 1$–0 and $J = 2$–1 transitions, μ_{CS} is the dipole moment of the CS molecule, T_{ex} is the excitation temperature, the T_{A} is the measured brightness temperature. The mass involved in the CS emission region is determined by

$$M(\mathrm{H_2}) = \left(\frac{\mu m_{\mathrm{H}}}{X_{\mathrm{CS}}}\right) \int N(\mathrm{CS}) ds\,, \quad (2)$$

where μ is the mean molecular weight (2.33 adopted in the following), m_{H} is the atomic mass unit, and X_{CS} is the fractional abundance of the CS molecule relative to H_2, which is adopted to be 2×10^{-9}. The integration is carried out over the CS emitting area. If we take $\mu_{\mathrm{CS}} = 1.96$ debye (Lovas & Krupenie 1974), V in kilometers per second, source distance D in parsecs, flux in janskys, then the above equation can be expressed in convenient units as

$$M(\mathrm{H_2}) = 2.4 \times 10^{-9}\left(\frac{D^2}{\mathrm{pc}^2}\right)\left(\frac{L_{\mathrm{CS}}}{\mathrm{Jy\ km\ s^{-1}}}\right)\left(\frac{T_{\mathrm{ex}}}{\mathrm{K}}\right) e^{7.05/T_{\mathrm{ex}}}\, M_{\odot}\,, \quad (3)$$

where the CS flux L_{CS} is the product of the flux density and the velocity range.

The excitation temperature of CS-emitting gas can be estimated from the CO temperature assuming a radially decreasing dependence. In the case of L1287, where the embedded infrared source may be the main heating source, the radial distribution of temperature can be examined in a simple way. It is further reasonable to assume that the temperature of gas is tightly related to that of dust, whose radial dependence is determined by the energy balance between emission and absorption. We write the dust emissivity law as $\kappa_\nu \sim \nu^{\alpha}$; then the radial temperature profile of dust is expected to be $T(r) \sim r^{-2/(4+\alpha)}$. We can roughly take the representative radius of CS to be about one-third that of CO, as estimated from the relative sizes of CO and CS outflows. Taking the observed CO temperature of 15 K, which also corresponds to the lower limit of the temperature, the expected excitation temperature of CS-emitting gas is 22 K if α is assumed to be 2. The upper limit of the CS excitation temperature is not expected to exceed the color temperature between the 60 μm and 100 μm bands of the *IRAS* source, which is 29 K for 00338+6312. The uncertainty in column density and hence mass estimation introduced by the temperature effect through the factor $T_{\mathrm{ex}}\, e^{7.05/T_{\mathrm{ex}}}$ is estimated to be $\leq 20\%$.

Equation (1) also omits the effect of finite optical depth, i.e., it does not take into account the reciprocal of the escape probability term, $\tau/(1 - e^{-\tau})$, for a finite optical depth τ. As τ ranges from 0.0 to 1.0, the derived column density may vary by a factor of 1.6. In the present case, the peak flux density, 0.4 Jy beam^{-1}, or 3.4×10^{-15} ergs s^{-1} cm^{-2} Hz^{-1} sr^{-1}, corresponds to a CS antenna temperature of 1.2 K. Utilizing the excitation temperature estimated above and assuming a filling factor of unity, we estimate the optical depth to be within 0.05–0.10, which therefore modifies the mass estimation through the escape probability term by 3%–5%, negligibly small compared with other factors. The above estimate of optical depth, although crude, makes us believe that outside the emission dip in the line profile, the CS $J = (2$–$1)$ emission is virtually optically thin.

No previous study on molecular abundance has been conducted toward L1287. The fractional abundance of CS, X_{CS}, is mostly in the range $(1$–$3) \times 10^{-9}$ in molecular clouds (e.g., Graedel, Langer, & Frerking 1982; Blake et al. 1987). In fact, an accurate value of this abundance cannot be specified toward a region even if one can measure with precision the CS column density. The abundance fluctuation which is commonly met prohibits a firm measure of the column density of molecular hydrogen, since the conversion from the column density of other species to hydrogen is indirect and thus uncertain. This in turn introduces the largest amount of uncertainty in estimating column density— in the most extreme case, one order of magnitude. In this paper we adopt X_{CS} to be 2×10^{-9}, a

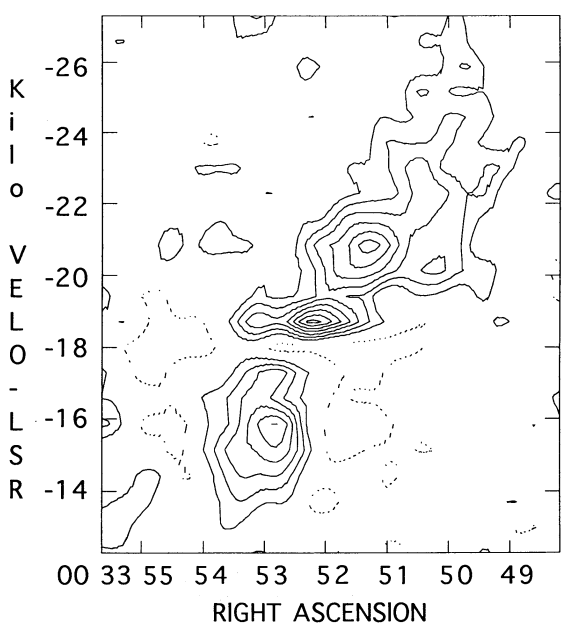

FIG. 4.—Position-velocity cut along the direction of the outflow at P.A. = 45°. Contour levels are arranged in the order 2.81×10^{-2} (-1.5, 1.5, 3.0, 4.5, 6.0, 7.5, 9.0) Jy beam^{-1}.

TABLE 1

PARAMETERS OF THE DENSE CS COMPONENTS

Component	Velocity Range (km s^{-1})	Size (pc × pc)	Flux (Jy km s^{-1})	Mass ($M_\odot$)
Red.....	(−12.00 to −15.00)	0.07 × 0.05	8.84	0.46
Disk.....	(−15.75 to −19.50)	0.08 × 0.06	22.69	1.18
Blue.....	(−20.25 to −27.75)	0.09 × 0.07	30.78	1.60

NOTE.—The velocity intervals of the three components are divided in accordance with those of ^{13}CO wings observed by Yang et al. 1991.

canonical value derived from several regions and consistent with chemical model calculations (see Blake et al. 1987 and references therein).

Again considering the emission minimum mentioned in § 3.1, which is more likely due to the missing-flux problem, one can expect the above way of mass estimation to reflect adequately small-scale features, including the outflow lobes and the localized low-velocity component near the center. The derived masses of the red, blue, and rest CS components are listed in the last column of Table 1. The total mass involved in the CS-emitting area in L1287 is 3.2 $M_\odot$. Masses of the redshifted and blueshifted components are obviously higher than those derived from the corresponding CO lobes from single-dish observations (Snell et al. 1990; Yang et al. 1991) and about a factor of 5–6 higher than those derived from HCO^+ (Yang et al. 1991). The uncertainty introduced by the abundance ratio of hydrogen to CS, as mentioned above, may be responsible for this large discrepancy. On the other hand, previous single-dish observations may be also limited by the unknown filling factor, suggested by the marginally resolved bipolar pattern of HCO^+ wings (see Fig. 8 in Yang et al. 1991).

4. DISCUSSION

4.1. *Comparison between the* CS *and Optical/Infrared Features*

Comparison of the CS emission with optical and infrared features provides useful information. The area of the CS emission and the optical nebula GN 00.33.9 in the *I*-band approximately coincide with each other, and both are elongated in the same direction at P.A. ~45°, suggesting that scattering of light by the dust mixed in the high-density CS gas results in the optical reflection nebula. In Figure 5 the low-velocity CS component is superimposed on the *I*-band emission by Staude & Neckel (1991). Neither RNO 1C nor RNO 1B coincides with the CS peak. Instead, these features, including RNO 1D, which is close to RNO 1C, appear in the inner part of the integrated CS map but do not correspond to any CS peak. Figure 5 indicates that there is no clear association of high-density clumps with RNO 1B and RNO 1C. The optical filament consisting of RNO 1B, RNO 1C, and RNO 1D occurs at the CS cavity and is aligned to the outflow axis.

Besides RNO 1B and RNO 1C, diffuse IR bipolar emission is detected in the region by Weintraub & Kastner (1993) and Kenyon et al. (1993). This diffuse emission, along with the outflow lobes, indicates that a cavity blown up by outflow gas exists around the young stellar objects in the L1287 cloud core. In tracing this bipolar extension, Weintraub & Kastner (1993) identified 00338+6312 as the illuminating source. Besides, the infrared streamer recognized from the images of Kenyon et al. (1993) suggests a certain degree of correspondence with the lower edges of the CS outflow. Such correspondence, although no clearer, is reminiscent of that between the CO outflow and the optical reflection nebula HH 102 in the case of L1551 (see

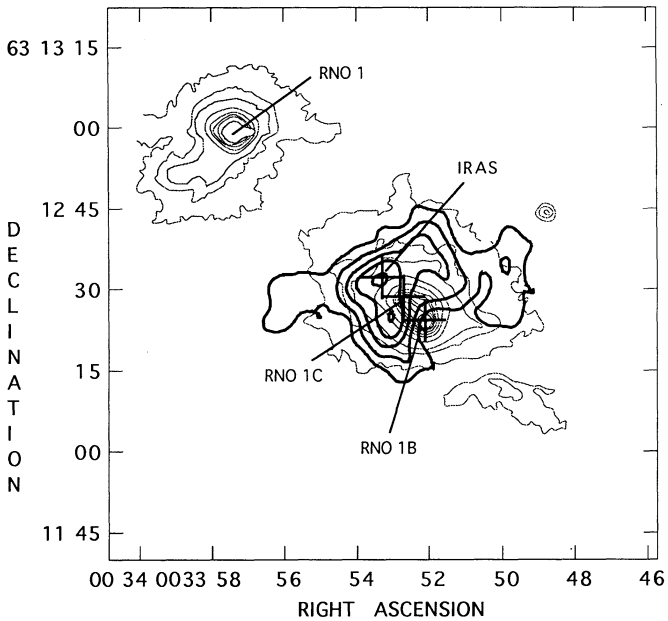

FIG. 5.—Overlay of the low-velocity CS component (see Fig. 2*b*), which is illustrated by the thick contours on the *I*-band optical emission from Staude & Neckel (1991) (*thin contours*).

Stocke et al. 1988), where reflection of light by the cavity of outflow results in a diffuse nebula.

The concavity of the CS disklike structure in Figure 2*b* (and Fig. 5) and the elongation of the nebula along the polar direction indicate that the depletion of dense gas occurs along the polar direction of the CS structure. This morphology suggests either that a disklike CS structure is responsible for creating the outflow, or, alternatively, that the CS structure results from the dynamic interactions of the parent molecular core with the outflow. Measured at the half-maximum level, the disk size is 20″, corresponding to 1.7 × 10^4 AU. Flattened, disklike structures around young stellar objects have been observed through interferometric observations, such as those associated with HL Tau and R Mon (Sargent & Beckwith 1987) and with protostellar sources in Taurus (Ohashi et al. 1991). These objects are revealed to have flattened molecular structures of 10^2–10^4 AU and masses of 0.1–1.0 $M_\odot$. Compared with these disks, the flattened CS disk in L1287 with a mass of 1.2 $M_\odot$ is among the massive ones.

4.2. *The Driving Source of the Molecular Outflow*

In the previous observations of CO outflow (Yang et al. 1991), we supposed that the driving source of the CO outflow is the *IRAS* source, and that the optical counterpart of this infrared source may be RNO 1. Owing to the higher precision in determining the positions of RNO 1, RNO 1B, and the *IRAS* source (Staude & Neckel 1991; Weintraub & Kastner 1993), RNO 1 should now be ruled out as the optical counterpart of IRAS 00338+6312. But the position error ellipse of the *IRAS* source, 28″ × 8″ at P.A. 40°, still extends over to include RNO 1C, RNO 1D, and marginally, RNO 1B.

The discovery of more than one young stellar object within the dense core region of L1287 makes the identification of the intrinsic driving source of the molecular outflow difficult. This difficulty is further amplified by the coincidental alignment of the young stellar objects along the outflow axis (see Fig. 1). Even so, some general arguments are valid for the driving

source. The clear bipolarity and the simple and regular shapes of the CS lobes from current observation, along with previous bipolar CO lobes, make us believe that the outflow in L1287 is powered by a single source. Outflows in the same direction of the CO and CS outflows driven by multiple sources are less feasible within the scope of available molecular line data.

In the observations at VLA, McCutcheon et al. (1991) marginally detected a continuum source at the position of the *IRAS* source with an upper limit of 0.22 mJy. The thermal radio source with a single-sided jet in the outflow direction, VLA 3, is more clearly revealed at 3.6 cm at VLA by Anglada et al. (1994). The position of the *IRAS* source is within 1″ of VLA 3 and 1″.5 of the predicted embedded source by Weintraub & Kastner (1993). If the radio source is the counterpart of the *IRAS* source, the same source which drives the thermal radio jet may be considered responsible for the CO/CS/HCO^+ outflow, a phenomenon frequently found toward outflow sources (see, e.g., Bieging, Cohen, & Schwarz 1984 for L1551; Rodríguez & Reipurth 1994 for HH 111; Anglada et al. 1994 and references therein). The presence of a single-sided radio jet and its elongation along the same direction of the molecular outflow may also support the possibility of the deeply embedded source as the driving source of the molecular outflow revealed from the region.

In Figure 6 the CS outflow gas is superimposed on the rest component of high-density gas. Apparently, RNO 1C is more symmetrically located with respect to the two outflow lobes than 00338+6312 and RNO 1B. But morphologically it is difficult to identify the driving source of the CS outflow, since the three young stellar objects, 00338+6312, RNO 1C, and RNO 1B are so closely located that the separations among them are significantly smaller than the overall sizes of the CS components. The difficulty is also partially due to the asymmetry of the two velocity lobes, with the blue lobe dominating

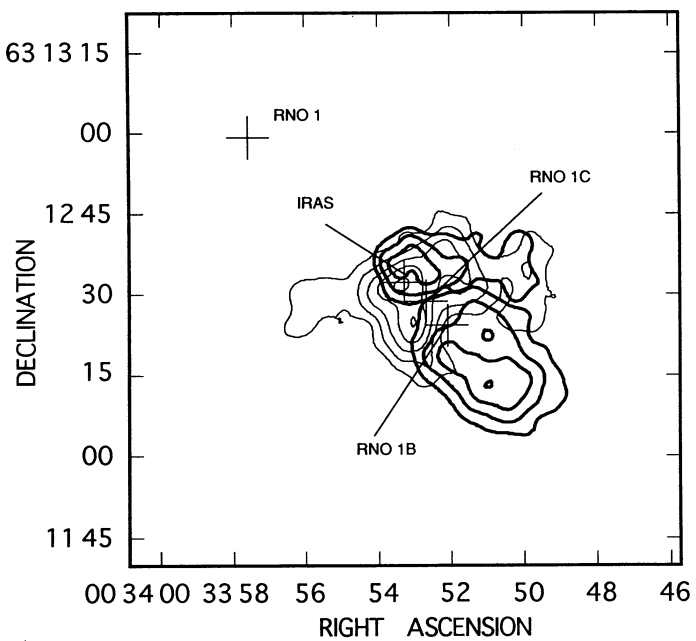

FIG. 6.—Mosaic of the three distinctive velocity components: the redshifted and the blueshifted components (*thick lines*) and the rest component (*thin contour lines*). The positions of the young stellar objects, IRAS 00338+6312, RNO 1B, and RNO 1C, are marked by crosses. The details are given in the text.

over the red one. Even so, it is still reasonable to expect that the driving source is associated with plenty of local high-density circumstellar gas. From this point of view, we can find that 00338+6312 is preferable for the driving source, since it is more deeply embedded than either RNO 1B or RNO 1C. Synthesizing the available molecular data, the near-infrared and optical data, and the radio continuum observations, we conclude that the most likely driving source of the outflow in L1287 is 00338+6312, which is almost identical to the illuminating source of the infrared nebula and VLA 3, the driving source of the radio jet. This identification is not exclusive and is worth future observations at higher resolutions in both infrared and millimeter wave bands.

Since RNO 1C and RNO 1D are within the error box of the *IRAS* source and RNO 1B is marginally included, it is likely that the *IRAS* luminosity is contributed by the multiple sources included in the large *IRAS* beam size. From the cataloged *IRAS* fluxes, one can estimate that the *IRAS* luminosities of FU Ori stars are in the range from 20 $L_\odot$ for L1551 IRS 5 to 104 $L_\odot$ for V1735 Cyg. Luminosities of the other FU Ori stars fall within this range, except that Z CMa and L1287 have higher *IRAS* luminosities. For Z CMa, a young binary system (Koresko et al. 1991), the luminosity contribution for the FU Ori counterpart cannot be unambiguously separated from its companion. Kenyon et al. (1993) supposed that most of the far-IR luminosity comes from RNO 1B/RNO 1C, in order to account for the optical luminosity. One may also speculate that a large fraction of the far-infrared luminosity in L1287 originates from the deeply embedded source if the far-IR luminosity is produced from the energy released during gas accretion. At any rate, precise determination of the relative contribution to the luminosities by the deeply embedded far-infrared source and its neighboring young stellar objects in L1287 cannot be made precisely based on available observations but relies on future observation.

4.3. *Implication for the Possible Outflow Models*

An apparent acceleration has been observed in the CS outflow in L1287. The emitting area of the CS outflow, 34″ × 20″, occupies only part of the CO outflow. The outflow velocity of the CS, which is within −28 to −12 km s^{-1}, is narrower than that of CO, −34 to −6 km s^{-1}. From these observations, it is understood that the outflow is composed of an outer CO flow of lower density and an inner CS flow of higher density. The co-appearance of CS and CO outflow may reflect a specific density structure, or density stratification, within outflow gas. This tendency suggests that, for a molecular outflow, the inner part does not need to be empty or to be a simple bubble structure, even though the more detailed density structure cannot be revealed by only limited lines of CO, HCO^+, or CS.

A quasi-linear dependence of outflow velocity on the distance from the central driving source is observed in L1287. This feature has been revealed from outflow sources by other molecular lines, such as CO from L1551 (Moriarty-Schieven & Snell 1988) and Orion B (Richer et al. 1992), and SiO from L1448 (Guilloteau et al. 1992).

The quasi-linear dependence of outflow velocity on distance has been found from a number of molecular outflows and has been interpreted by models such as the swept-up shell or jet-driven outflows (e.g., Shu et al. 1991; Masson & Chernin 1993). Under the picture of a swept-up shell, the velocity, V_s, of the swept-up shell moving inside a radially decreasing ambient gas

with a density profile $\rho(r) \sim r^{-\beta}$ is expected to depend linearly on the radial distance r through the relation $V_s/r = 2/(4 + \beta)t$ (see Cabrit 1993). Assuming that the outflow gas in L1287 is propagating within an isothermal molecular cloud core which has a radial density profile of $\beta = 2$ (Shu 1977), from the scale of the blue lobe, 35″, and its velocity span of 8 km s^{-1}, we estimate in this way that the age of the high-density flow should be 6×10^3 yr, which is about half of that derived from CO (Yang et al. 1991) and implies that the dense CS outflow has been initiated later than the CO outflow. Since the inclination angle of the source along the line of sight is estimated to be ~45°, it has little effect on the above discussion.

The existence of high-density CS clumps further indicates that the outflow gas is nonuniform. Such clumpiness shares a similarity to that revealed recently in CO at L1448 (Bachiller et al. 1990) and VLA 1623 (André et al. 1990) and in SiO at L1448 (Bachiller, Martín-Pintado, & Fuente 1991). The short dynamic timescale implied by the CS flow also suggests that high-density molecular clumps may be formed at the epoch as soon as the entrained gas is blown out from the central engine. It can be recognized that the CS clumps have a broader line width (~2 km s^{-1} from the multivelocity maps in Fig. 3), which implies that these clumps are highly disturbed. This is distinguished with either the quiescent HCO^+ cloudlets found in the HH 7–11 system (Rudolph & Welch 1988) or the ammonia clumps from HH 1/2 (e.g., Torrelles et al. 1992).

The apparent acceleration starts from the innermost part of the outflow as suggested by the relative geometry of CO and CS. It is evident in this case that the terminal velocity of CS clumps is lower than that of CO during the past acceleration motion, although it is not clear whether the CS clumps can finally gain higher velocities to develop into the bullets as observed in L1448 and other outflow sources in CO.

5. CONCLUSIONS

The following points conclude this study:

1. Interferometric observations have been made toward the infrared source in L1287 with a resolution of 8.″0 × 6.″4. Strong CS emission of 34″ × 20″ has been detected from the central portion of the L1287 molecular cloud core.

2. The CS emission appears over a velocity range as broad as 16 km s^{-1} and shows a well-separated pattern of bipolar outflow. The dynamic timescale of the CS outflow, 8×10^3 yr, is shorter than that indicated by the corresponding CO outflow. The dense outflow gas exhibits condensations of smaller sizes and demonstrates a quasi-linear dependence of velocity on distance, which characterizes an apparent acceleration tendency.

3. The CS emission generally coincides with the optical nebula associated with RNO 1B and RNO 1C. The emission peak, within 1″ of the thermal radio source found by Anglada et al. (1994), coincides not with either RNO 1B or RNO 1C but with the *IRAS* source. The low-velocity CS emission outlines a flattened structure perpendicular to the outflow with the cold *IRAS* source located in the center. The three optical maxima, RNO 1B, RNO 1C, and RNO 1D, are located within the cavity of low-velocity CS gas and are approximately aligned along the outflow axis. Cumulative evidence prefers the deeply embedded *IRAS* source to be the driving source of the molecular outflow in L1287.

4. No significant continuum emission has been detected at the frequency of 98 GHz, suggesting that little thermal dust emission is generated from the circumstellar materials around the deeply embedded young stellar object.

The authors are indebted to staff members at RNO for their help in conducting interferometric observations. They benefited from fruitful discussions with M. Ishiguro, R. Kawabe, K. Morita, K. Tatematsu, T. Umemoto, S. Ishizuki, and C.-P. Liu. They acknowledge G. Anglada and J. Kastner for earlier communication of their results. The authors also appreciate the helpful comments from the referee. J. Y. acknowledges support from the S.-s. Huang Astrophysical Foundation, NNSFC grants, and the State Education Commission. He also thanks NRO for providing partial support for this work.

REFERENCES

André, P., Martín-Pintado, J., Despois, D., & Montmerle, T. 1990, A&A, 236, 180
Anglada, G., Rodríguez, L. F., Girart, J. M., Estalella, R., & Torrelles, J. M. 1994, ApJ, 420, L91
Bachiller, R., Cernicharo, J., Martín-Pintado, J., Taffala, M., & Lazareff, B. 1990, A&A, 231, 174
Bieging, J. H., Cohen, M., & Schwartz, P. R. 1984, ApJ, 282, 699
Blake, G. A., Sutton, E. C., Masson, C. R., & Phillips, T. G. 1987, ApJ, 315, 621
Cabrit, S. 1993, in Star Formation and Techniques in Infrared and Millimeter-Wave Astronomy, ed. T. P. Ray & S. V. W. Beckwith (Berlin: Springer-Verlag), 1
Fukui, Y. 1989, in Low Mass Star Formation and Pre–Main Sequence Objects, ed. B. Reipurth (Garching: ESO), 95
Graedel, T. E., Langer, W. D., & Frerking, M. A. 1982, ApJS, 48, 321
Guilloteau, S., Bachiller, R., Fuente, A., & Lucas, R. 1992, A&A, 256, L49
IRAS Point Source Catalog, Version 2. 1988, Joint *IRAS* Science Working Group (Washington, DC: GPO)
Kenyon, S. J., Hartmann, L., Gomez, M., Carr, J. S., & Tokunaga, A. 1993, AJ, 105, 1505
Koresko, C. D., Beckwith, S. V. W., Ghez, A. M., Matthews, K., & Neugebauer, G. 1991, AJ, 102, 2073
Lovas, F. J., & Krupenie, P. H. 1974, J. Phys. Chem. Ref. Data, 3, 245
Masson, C. R., & Chernin, L. M. 1993, ApJ, 414, 230
McCutcheon, W. H., Dewdney, P. E., Purton, C. R., & Sato, T. 1991, AJ, 101, 1435
Moriarty-Schieven, G. H., & Snell, R. L. 1988, ApJ, 332, 364
Ohashi, N., Kawabe, R., Hayashi, M., & Ishiguro, M. 1991, AJ, 102, 2054
Richer, J. S., Hills, R. E., & Padman, R. 1992, MNRAS, 254, 525
Rodríguez, L. F., & Reipurth, B. 1994, A&A, 281, 882
Rudolph, A., & Welch, W. J. 1988, ApJ, 326, L31
Sargent, A. I., & Beckwith, S. 1987, ApJ, 323, 294
Shu, F. H. 1977, ApJ, 214, 488
Shu, F. H., Ruden, S. P., Lada, C. J., & Lizano, S. 1991, ApJ, 370, L31
Snell, R. L., Dickman, R. L., & Huang, Y.-L. 1990, ApJ, 352, 139
Staude, H. J., & Neckel, Th. 1991, A&A, 244, L13
Stocke, J. T., Hartigan, P. M., Strom, S. E., Strom, K. M., Anderson, E. R., Hartmann, L., & Kenyon, S. 1988, ApJS, 68, 229
Torrelles, J. M., Rodríguez, L. F., Cantó, J., Anglada, G., Gómez, J. F., Curiel, S., & Ho, P. T. P. 1992, ApJ, 396, L95
Weintraub, D. A., & Kastner, J. 1993, ApJ, 411, 767
Yang, J., Umemoto, T., Iwata, T., & Fukui, Y. 1991, ApJ, 373, 137